



High-pressure behaviour and elastic constants of 1M and 2M1 polytypes of phlogopite $\text{KMg}_3\text{Si}_3\text{AlO}_{10}(\text{OH})_2$

Gianfranco Ulian¹, Francesca Ranellucci¹, Giovanni Valdrè¹

¹Dipartimento di Scienze Biologiche, Geologiche e Ambientali, Università di Bologna “Alma Mater Studiorum”, Plesso di Mineralogia, Piazza di Porta San Donato 1, 40126 Bologna, Italy

Correspondence to: Giovanni Valdrè (giovanni.valdre@unibo.it)

Abstract. In the present work, the elastic properties of both 1M and 2M1 phlogopite polytypes, $\text{KMg}_3\text{Si}_3\text{AlO}_{10}(\text{OH})_2$ (monoclinic crystal system) were investigated from *PV* equation of state fitting and by analysis of the fourth-rank elastic tensor. The analysis was performed within the Density Functional Theory framework, using all-electron Gaussian-type orbitals basis sets and the B3LYP functional corrected a posteriori to include long-range interactions (B3LYP-D*). In general, the elastic properties of the two polytypes were strongly anisotropic, with the axial moduli ratio $M(a) : M(b) : M(c)$ being close to 4 : 4 : 1. The volume-integrated third-order Birch-Murnaghan equation of state fitting parameters at 0 K were $K_0 = 57.9(2)$ GPa, $K' = 8.29(7)$ and $V_0 = 489.82(3)$ Å³ for phlogopite-1M, which were very close to those of the 2M1 polytype, i.e., $K_0 = 58.3(1)$ GPa, $K' = 8.71(8)$ and $V_0 = 978.96(9)$ Å³. The monoclinic elastic tensors obtained for the two polytypes of phlogopite, which have never been experimentally reported for both minerals so far, were in line with the *PV* behaviour of the mineral, providing further data related to the directional dependence of the elastic properties and seismic wave propagation. The elastic properties from both *PV* hydrostatic compression and from the elastic moduli tensor were discussed against the available experimental and theoretical data in the scientific literature, extending the knowledge on this important trioctahedral phyllosilicate.

1 Introduction

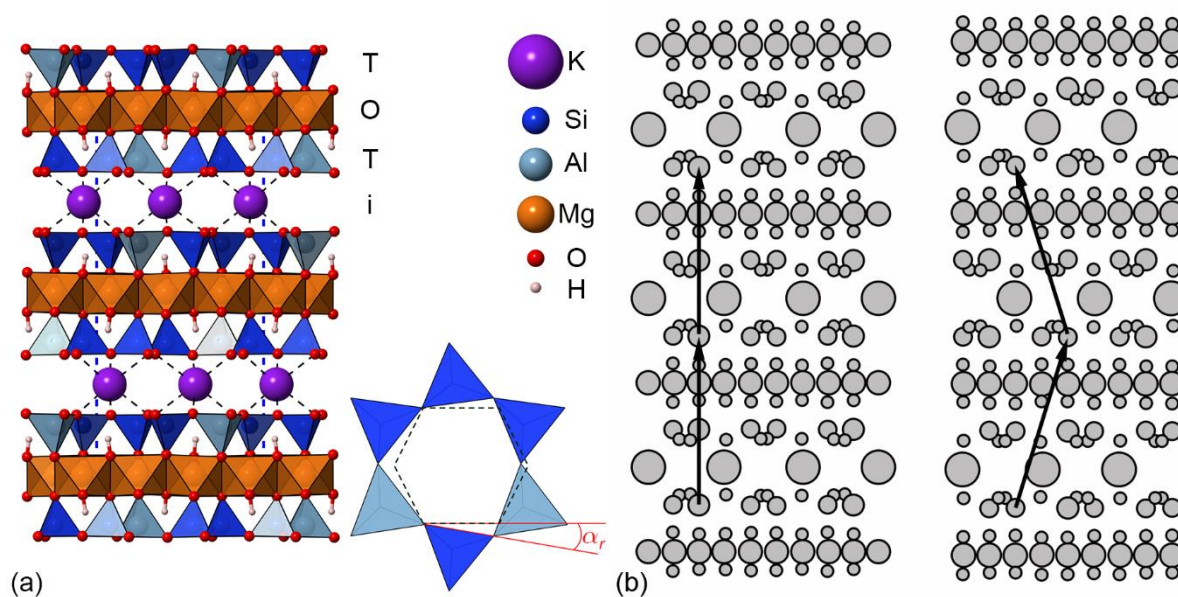
Phlogopite [commonly abbreviated with Phl, $\text{K}(\text{Mg},\text{Fe})_3\text{Si}_3\text{AlO}_{10}(\text{OH})_2$, with Mg/Fe ratio greater than 2], is a ubiquitous mica mineral that can be found in different geological environments and pressure-temperature conditions, i.e. igneous, sedimentary, and metamorphic rocks (Icenhower and London, 1995; Trønnes, 2002), and one of the water and potassium reservoirs in the Earth's mantle (Virgo and Popp, 2000; Tutti et al., 2000).

From the crystallographic point of view, like other phyllosilicates, phlogopite is made of a 2:1 layer formed by two tetrahedral sheets (labelled as T) that sandwich an octahedral one (O). These T-O-T (or TOT) layers present strong (covalent/ionic) in-plane bonds and a negative charge because of $\text{Al}^{\text{III}}/\text{Si}^{\text{IV}}$ substitutions in the T sheets, which is balanced by potassium cations in the interlayer. Thus, the structure is held together along the *c* crystallographic axis by a mix of Coulombic (electrostatic) and weak (van der Waals) interactions (Ventrucci et al., 2009). Phlogopite presents different



30 polytypes due to different arrangement of the TOT layers along the [001] direction, with the $1M$ and the $2M_1$ being the most common in nature both belonging to the monoclinic crystal system (Lacalamita et al., 2012), while a third polytype, $3T$ (trigonal), is known to be very rare (Gatta et al., 2011). A graphical representation of the most common polytypes is shown in Fig.1.

Phlogopite is also a widely adopted mineral in the technological field, for instance in the manufacture of ceramics and
 35 glasses (King et al., 2000; Ariane et al., 2023) and, more recently, gained attention as a potential dielectric (insulating) material for optical and electronic applications because it presents a band gap of ca. 5–6 eV that can be modulated by microchemical variations, e.g., by Fe^{II}/Mg^{II} substitutions (Ulian and Valdrè, 2023a).



40 **Figure 1. (a) Structural model of the phlogopite- $2M_1$ model viewed along the [100] direction. In the bottom right corner, a graphical representation of the tetrahedral rotation angle α_r is shown. (b) Schematic view of the stacking of the TOT layers in the $1M$ (left) and $2M_1$ (right) polytypes. The black arrows link two points related by symmetry.**

For both geological and technological applications, it is also important to know the elastic properties of this mineral to understand and explain geophysical observations in subduction zones and devise new uses of phlogopite, respectively. Many
 45 experimental studies were focused on the equation of state of phlogopite (Pavese et al., 2003; Comodi et al., 2004; Gatta et al., 2011), but mainly on the $1M$ polytype. As also observed by Chheda et al. (2014), no measurement of the full monoclinic elastic constant tensor has ever been reported in the scientific literature. The only experimental evidence of this elastic property is related to elastic wave propagation (EWP) experiments that provided just the 5 independent constants, considering the mineral as pseudo-hexagonal (Aleksandrov et al., 1974; Alexandrov and Ryzhova, 1961). The full elastic
 50 tensor of phlogopite- $1M$ was only recently provided from *ab initio* simulations within Density Functional Theory (DFT) at the local density approximation (LDA) and generalized gradient approximation (GGA) levels (Chheda et al., 2014).



However, the authors did not employ any correction to include long-range interactions in the physical treatment of phlogopite. Furthermore, no studies on the elastic properties of phlogopite- $2M_1$ were ever carried out and reported.

For all these reasons, the present work is focused on the elastic properties of phlogopite, considering both $1M$ and $2M_1$ polytypes. To this aim, *ab initio* DFT simulations were performed (i) to understand the compressional behaviour of the mineral through an equation of state fitting, (ii) to obtain the full monoclinic elastic moduli and (iii) to assess the role of polytypism on the elastic behaviour of phlogopite. All the data were compared and discussed with both experimental and theoretical results found in the scientific literature to extend the knowledge on this important phyllosilicate.

2 Computational Methods

As previously introduced, the simulations reported in the present work were carried out within the Density Functional Theory framework. In detail, the hybrid B3LYP functional (Becke, 1993;Lee et al., 1988), which includes 20% of exact Hartree-Fock exchange and some non-local contribution to the exchange-correlation terms, was employed throughout the present study. B3LYP is considered a suitable choice when dealing with the simulation of the structural and elastic properties of minerals due to its high accuracy, and it was already adopted with success for the description of several other minerals (Prencipe et al., 2009;Ottonello et al., 2010;Belmonte, 2017;Ulian and Valdrè, 2023b;Ulian and Valdrè, 2019) and phlogopite (Ulian and Valdrè, 2023a). However, since most generalized-gradient approximation functionals, including their hybrid counterparts, do not adequately include van der Waals (long-range) interactions, the DFT-D2 correction (Grimme, 2006) was adopted, employing the parameters of Civalleri and co-workers (2008) for the B3LYP functional (B3LYP-D* method). The all-electron Gaussian-type orbitals (GTO) used to construct the Kohn-Sham orbitals within the linear combination of atomic orbitals (LCAO) approach were the same used in a recent work on the $1M$ polytype of phlogopite (Ulian and Valdrè, 2023a). Si, Al, Mg, K, O and H atoms were described with 88-31G* (Nada et al., 1996), 85-11G* (Catti et al., 1994), 8-511d1G (Valenzano et al., 2007), 86-511G (Dovesi et al., 1991), 8-411d11G (Valenzano et al., 2007), and 3-1p1G (Gatti et al., 1994), respectively.

The accuracy of the Coulomb and exchange series were controlled by five thresholds set to 10^{-8} (ITOL1 to ITOL4) and 10^{-16} (ITOL5) for the structural relaxation procedures, whereas the convergence on the total energy was set to 10^{-8} Hartree. The reciprocal space was sampled with a $5 \times 5 \times 5$ Monkhorst–Pack mesh (Monkhorst and Pack, 1976), corresponding to 39 independent k points.

The lattice and internal geometry were optimized within the same run using a numerical gradient for the unit cell parameters and an analytical gradient for the atomic positions. The Hessian matrix was upgraded with the BFGS algorithm (Broyden, 1970a, b;Fletcher, 1970;Goldfarb, 1970;Shanno, 1970). The tolerances for the maximum allowed gradient and the maximum atomic displacement were set to 10^{-5} Ha bohr $^{-1}$ and 4×10^{-5} bohr, respectively.



All the simulations were performed with the CRYSTAL17 code (Dovesi et al., 2018), whereas the QUANTAS software (Ulian and Valdrè, 2022, 2024) was employed to post-process the elastic data. Graphical representations have been carried out with the molecular graphics program VESTA (Momma and Izumi, 2008).

85 3. Results and discussion

3.1 2M₁-Phlogopite crystal structure

The initial model of the crystal structure of 2M₁- phlogopite was created from the single-crystal X-ray diffraction data of Lacalamita et al. (2012), which was subsequently optimized within the B3LYP-D* level of theory. The mineral belongs to the monoclinic system (space group *C2/c*) presenting two independent tetrahedral sites (labelled as T) and two octahedral sites (M), with partial occupancies of the cationic sites with several possible atoms. For example, the TO₄ tetrahedral sites in the unit cell are generally occupied by about 70% by Si and 30% by Al (Laurora et al., 2007;Lacalamita et al., 2012), which can be translated in 1/4 sites being randomly occupied by aluminium. However, as also explained in a previous study on the 1M polytype (Ulian and Valdrè, 2023a), theoretical modelling requires each site being deterministically occupied by a single kind of atom; in the example cited above, a T site could present either Al or Si but not by both at the same time. Thus, to preserve the monoclinic lattice of phlogopite when the Al^{III}/Si^{IV} substitutions are included in the structure, the 2M₁ polytype with formula KMg₃(AlSi₃)O₁₀(OH)₂ was described with the *P2/c* space group (23 inequivalent atoms, 88 atoms in the unit cell, *Z* = 4 unit formulas), which is a sub-group of the *C2/c* symmetry. Within the *P2/c* space group, phlogopite-2M₁ presented four inequivalent T sites (Si^{IV} in T1–T3, Al^{III} in T4) and three non-equivalent O sites (M1–M3). Hence, each T site was related to four SiO₄ or AlO₄ tetrahedra, whereas all octahedral sites are related to two MgO₆ octahedra. Table 1 reports the lattice parameters, tetrahedral (T_{thick}) and octahedral (M_{thick}) sheet thicknesses, interlayer distance (I_{thick}), and selected polyhedral properties, alongside previous XRD refinements.

The simulations are in good agreement with the experimental crystallographic data reported in literature, showing a small underestimation of the unit cell volume ($\Delta V = -1.0\%$), which is the result of a slight expansion of the tetrahedral and octahedral sheet thicknesses ($\Delta T_{\text{thick}} = 1.5\%$ and $\Delta O_{\text{thick}} = 1.8\%$, respectively) and a contraction of the interlayer distance ($\Delta I_{\text{thick}} = -2.5\%$). These results for the 2M₁-phlogopite are in agreement with previous simulations of the 1M polytype (Ulian and Valdrè, 2023a) and other phyllosilicates and layered minerals (Ulian et al., 2013;Ulian and Valdrè, 2015a, b;Ulian and Valdrè, 2019), where the inclusion of long-range interactions in the physical treatment is of utmost importance to properly simulate the crystal-chemistry and properties of this kind of structures.



Table 1. Equilibrium geometry of $2M_1$ -phlogopite as obtained from DFT/B3LYP-D*, compared to previous experimental refinements.

$2M_1$ polytype	B3LYP-D*	XRD ^a	SC-XRD ^b
space group	<i>P2/c</i>	<i>C2/c</i>	<i>C2/c</i>
<i>a</i> (Å)	5.2977	5.3332	5.3236
<i>b</i> (Å)	9.1918	9.2376	9.2217
<i>c</i> (Å)	20.1591	20.069	20.2039
β (°)	94.732	95.125	95.078
<i>V</i> (Å ³)	978.30	984.77	987.97
<i>T</i> _{thick} (Å)	2.2722	2.268	2.239
<i>M</i> _{thick} (Å)	2.1783	2.128	2.140
<i>I</i> _{thick} (Å)	3.3225	3.330	3.406
TQE			
T1(Si1)	1.0016		1.000
T2(Si2)	1.0015		1.000
T3(Si3)	1.0015		
T4(Al1)	1.0012		
mean	1.0015		1.000
Volume T (Å ³)			
T1(Si1)	2.2520		2.329
T2(Si2)	2.2655		2.329
T3(Si3)	2.2510		
T4(Al1)	2.7572		
mean	2.3814		2.329
OQE			
M1(Mg1)	1.0091		1.012
M2(Mg2)	1.0084		1.011
M3(Mg3)	1.0097		
mean	1.0091		1.012
Volume O (Å ³)			
M1(Mg1)	11.7940		11.84
M2(Mg2)	11.8017		11.62
M3(Mg3)	11.7593		
mean	11.7850		11.73

Notes: a – X-ray diffraction data of Laurora et al. (2007); b – single-crystal XRD refinement of Lacalamita et al. (2012) performed on sample BU1_14. *T*_{thick}, *M*_{thick}, and *I*_{thick} are tetrahedral sheet thickness (calculated from the *z* coordinates of the basal and apical oxygen atoms), the octahedral sheet thickness (calculated from the *z* coordinates of the apical and hydroxyl O atoms) and interlayer thickness (calculated from the *z* coordinates of the basal oxygen atoms), respectively. TQE and OQE are the tetrahedral and octahedral quadratic elongations, respectively (Robinson et al., 1971). T and M represent the generic tetrahedral and octahedral sites, respectively.

3.2 Compressional behaviour of phlogopite 1M and $2M_1$ polytypes

The compressional behaviour of phlogopite was modelled considering different unit-cell volumes, both smaller (compressed) and larger (expanded) with respect to the equilibrium geometry volume (*V*_{eq}). Then, the internal coordinates and lattice parameters were optimized keeping the selected volume fixed during the procedure, constraining the space group of 1M-phlogopite (*P2*) and $2M_1$ -phlogopite (*P2/c*), a procedure known as “symmetry preserving, variable cell-shape structure relaxation” that was proposed by Pfrommer and collaborators (1997). The equilibrium geometry of 1M-phlogopite was



125 retrieved from the work of Ulian and Valdrè (2023a) that was obtained with the same computational settings here adopted for the $2M_1$ polytype.

The dependence of the total energy E of the mineral at the different volumes V , i.e., the $E(V)$ curve, was described in terms of a volume-integrated 3rd-order Birch-Murnaghan equation of state, BM3 (Birch, 1947), as reported by Hebbache and Zemzemi (2004):

$$130 \quad E = E_0 + \frac{9}{16} K_0 V_0 \left\{ K' (\eta^2 - 1)^3 + [(\eta^2 - 1)^2 (6 - 4\eta^2)] \right\} \quad (1)$$

$$\eta = \left(\frac{V_0}{V} \right)^{1/3} \quad (2)$$

where η is a dimensionless parameter called dilaton, K_0 is the bulk modulus at 0 K, K' its pressure first derivative and V_0 the volume at zero pressure. The pressure values at each unit cell volume (reported in Table 2) were calculated using the fitting parameters K_0 , K' and V_0 obtained from the previous equation and employed in the well-known P-V formulation of the BM3

135 (Birch, 1947):

$$P = P_0 + \frac{3}{2} K_0 (\eta^7 - \eta^5) \left\{ 1 - \frac{3}{4} (4 - K') (\eta^2 - 1) \right\} \quad (3)$$

with P_0 the reference pressure (0 GPa). In Table 3, the BM3 equation of state parameters for both 1M and $2M_1$ phlogopite are reported. A graphical representation of the volume and axis lengths as a function of calculated pressure is presented in Fig.2. In general, there is a fine agreement between the relative variation of the cited structural properties obtained from the present theoretical simulations and the experimental ones from X-ray diffraction (Comodi et al., 2004; Pavese et al., 2003).

140

Table 2. Equation of state parameters and associated standard deviations (σ) obtained for the 1M and $2M_1$ polytypes of phlogopite.

Polytype	K_0 (GPa)	σ_{K_0} (GPa)	K'	$\sigma_{K'}$	V_0 (Å ³)	σ_{V_0} (Å ³)	Method	Reference
1M	57.9	0.2	8.29	0.07	489.82	0.03	GTO/B3LYP-D*	present work
$2M_1$	58.3	0.1	8.71	0.08	978.96	0.09	GTO/B3LYP-D*	present work
1M	54	2	7	1	497.1	0.1	SCXRD	Comodi et al. (2004)
1M	48.1	1.1	9.0	0.3	489.1	0.3	SXRPD	Pavese et al. (2003)
1M	59	2	-	-	487.7	0.2	SCXRD	Hazen and Finger (1978)
1M	60.8	4.3	8.1	1.7	473.03	1.06	PAW/LDA	Chheda et al. (2014)
1M	41.6	2.5	10.1	1.3	518.72	1.08	PAW/GGA	Chheda et al. (2014)

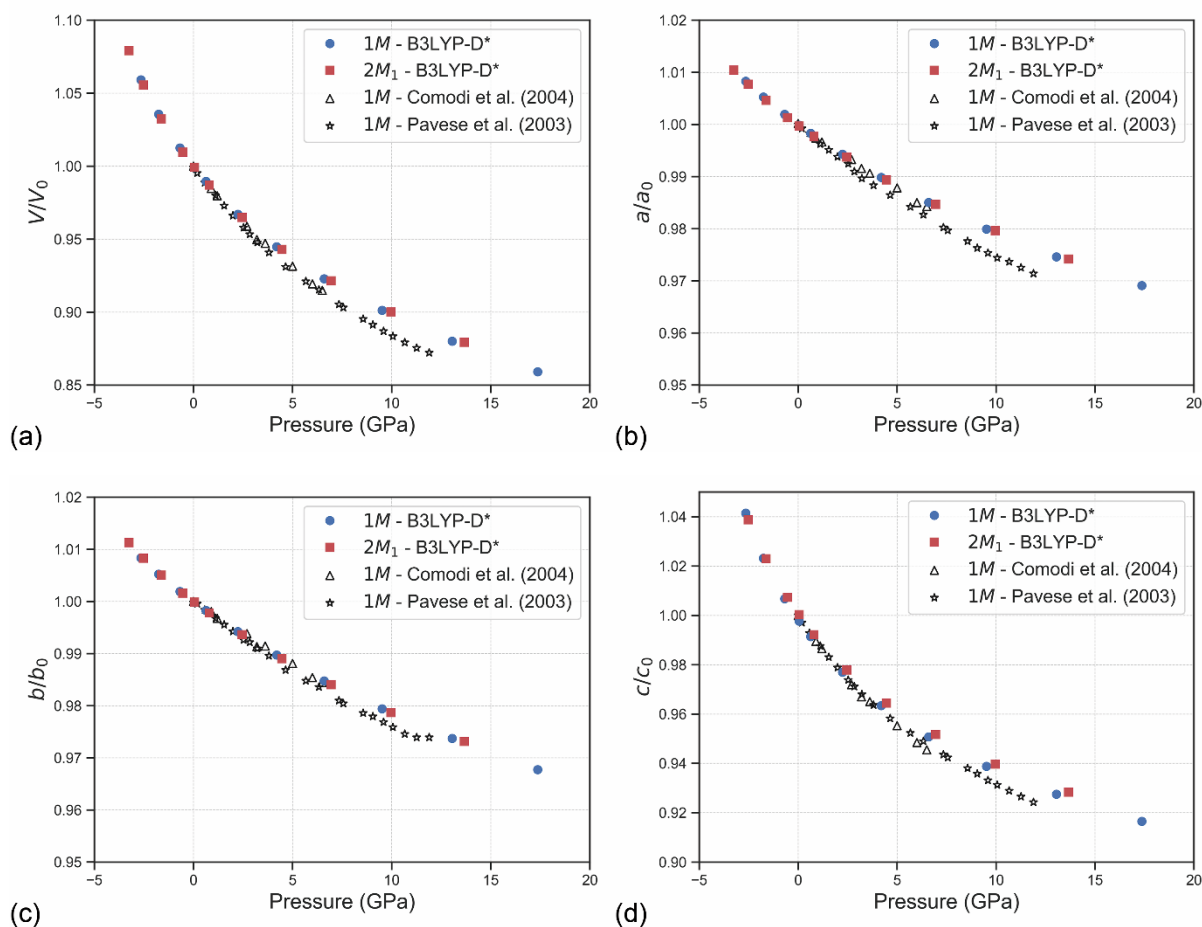
Notes: GTO – Gaussian-type orbitals; PAW – projector-augmented wave; SCXRD – single-crystal X-ray diffraction; SXRPD – synchrotron X-ray powder diffraction.

145

The axial compressibility, M_0 , was obtained using a linearized form of the third-order Birch-Murnaghan equation of state, as described by Angel et al. (2014), which was also employed to re-calculate the experimental compressibility reported by Pavese et al. (2003) and Comodi et al. (2004) including the uncertainties on pressure and lattice parameters. The results are shown in Table 3, alongside the theoretical results of Chheda and collaborators (2014). The results are consistent for all the simulations, as the bulk modulus $K_0 = [M_0^{-1}(a) + M_0^{-1}(c) + M_0^{-1}(c)]$ calculated from the axial compressibility is within 2.64% (1M) and 1.67% ($2M_1$) from the K_0 value obtained from the equation of state fit. Similar figures were calculated by

150

Chheda et al. (2014) and Pavese et al. (2003), and the recalculated values of Comodi et al. (2004) with the linearized formulation lead to a bulk modulus within 0.57% the value obtained from the PV EoS fitting.



155

Figure 2. Evolution of (a) unit cell volume V/V_0 , (b) a/a_0 , (c) b/b_0 and (d) c/c_0 as a function of pressure for the phlogopite polytypes $1M$ and $2M_1$. The experimental data of Pavese et al. (2003) and Comodi et al. (2004) are reported for a comparison.

Table 3. Axial compressibility parameters obtained from linearized equation of state fit.

Polytype	GTO/B3LYP-D* ^a		SXRPD ^b	SCXRD ^c	PAW/LDA ^d	PAW/GGA ^d
	$1M$	$2M_1$	$1M$	$1M$	$1M$	$1M$
a_0 [Å]	5.2992(1)	5.2999(3)	5.314(1)	5.336(1)	5.238(7)	5.360(3)
$M_0(a)$ [GPa]	344(5)	359(3)	290(10)	362(28)	395(21)	274(15)
$M'(a)$	32(1)	30(1)	24(3)	13(9)	-	-
b_0 [Å]	9.1960(4)	9.1920(4)	9.201(3)	9.240(3)	9.086(7)	9.298(5)
$M_0(b)$ [GPa]	354(3)	344(1)	312(12)	401(59)	406(20)	281(14)
$M'(b)$	25(1)	29(1)	24(3)	9(6)	-	-
c_0 [Å]	10.214(5)	20.150(9)	10.153(3)	10.238(6)	10.200(7)	10.590(32)
$M_0(c)$ [GPa]	77(3)	85(2)	72(2)	76(7)	84(25)	61(17)
$M'(c)$	24(1)	21(1)	18(1)	15(4)	-	-

Notes: a – present work; b – Pavese et al. (2003); c – Comodi et al. (2004); d – Chheda et al. (2014). GTO – Gaussian-type orbitals; PAW – projector-augmented wave; SCXRD – single-crystal X-ray diffraction; SXRPD – synchrotron X-ray powder diffraction.

160



Crystal structure data of both $1M$ and $2M_1$ polytypes are reported in Tables S1 and S2 (Supplementary Materials), respectively, providing further insights into the pressure effects on the phlogopite internal geometry.

The TO_4 tetrahedra showed a stiff behaviour, with zero-pressure bulk moduli equal to 282(3) GPa and 285(2) GPa for the $1M$ and $2M_1$ polytypes, respectively, whereas the octahedral MO_6 units were more compressible, presenting a bulk modulus of 143(1) GPa for both phlogopite polytypes (Fig.3a). This means that the TOT layer of the two minerals presented similar elastic properties. As also explained in previous works on phyllosilicates (Comodi et al., 2004; Chheda et al., 2014; Ulian and Valdrè, 2015c), the variation of the tetrahedral rotation angle α_r (Donnay et al., 1964b, a) is the main mechanism that accommodated the compression of the mineral. The α_r value is greater than 0 for both phlogopite polytypes at equilibrium, which means that the TO_4 mesh is not hexagonal (ideal) but forms a di-trigonal ring (see Fig.1), and α_r increases with pressure as reported in Fig.3b. This trend is in line with the simulations performed by Chheda and collaborators (2014), and with the general compressional behaviour of trioctahedral micas reported by several authors (Comodi and Zanazzi, 1995; Gatta et al., 2015; Gatta et al., 2011; Pavese et al., 1999; Pavese et al., 2003; Pawley et al., 2002). In addition, it is interesting to note that the octahedral flattening angle ψ became smaller by increasing pressure in the $1M$ polytype, whereas a direct proportionality was observed for the $2M_1$ one.

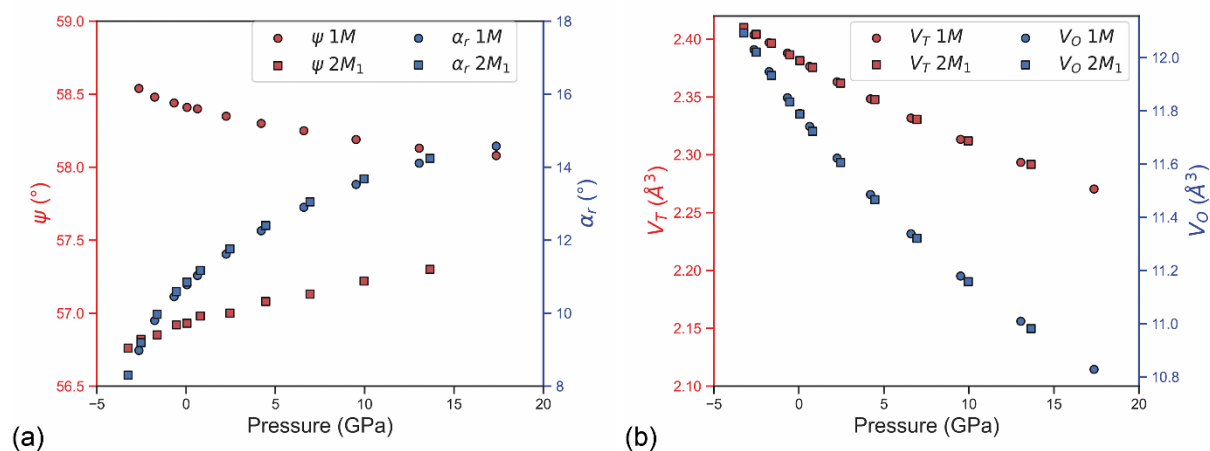


Figure 3. (a) Variation as a function of pressure of the octahedral flattening angle ψ (red symbols) and tetrahedral rotation angle α_r (blue symbols) in the $1M$ and $2M_1$ phlogopite models. (b) Evolution of the tetrahedral TO_4 and octahedral MO_6 polyhedral volume with pressure.



3.3 Elastic constants and derived quantities

To provide a complete analysis of the elastic behaviour of phlogopite polytypes, the second-order elastic tensor of the two models was also calculated. The approach relies on stress-strain relationships based on total energy $E(V, \varepsilon)$ calculations through a Taylor expansion in terms of the strain components truncated at the second order:

$$E(V, \varepsilon) = E(V_0) + V \sum_{\alpha} \sigma_{\alpha} \varepsilon_{\alpha} + \frac{V}{2} \sum_{\alpha\beta} C_{\alpha\beta} \varepsilon_{\alpha} \varepsilon_{\beta} + \dots \quad (4)$$

where ε is the strain, σ is the stress, \mathbf{C} is the 6×6 matrix representation of the elastic tensor (Voigt's notation), V is the volume of the strained unit cell and V_0 is the volume at equilibrium. In this expression, $\alpha, \beta = 1, 2, 3, \dots, 6$. The adiabatic second-order elastic moduli are related to the second derivatives of the total energy E on the strain according to:

$$C_{\alpha\beta} = \left. \frac{1}{V} \frac{\partial^2 E}{\partial \varepsilon_{\alpha} \partial \varepsilon_{\beta}} \right|_0 \quad (5)$$

The $C_{\alpha\beta}$ values were calculated by imposing a certain amount of strain ε along the crystallographic direction corresponding to the component of the dynamical matrix. This procedure is automated in the CRYSTAL code under the keyword ELASTCON (Perger et al., 2009), and in the present simulations the default values that control the calculation of the elastic moduli were employed. To calculate the elastic tensor, the crystal was oriented with the **b** and **c** crystallographic axes parallel to the *y* and *z* Cartesian axes, respectively. Within this crystal orientation and considering the monoclinic lattice, the 6×6 matrix \mathbf{C} of the elastic moduli in Voigt's notation is given by:

$$\mathbf{C} = \begin{pmatrix} C_{11} & C_{12} & C_{13} & 0 & C_{15} & 0 \\ & C_{22} & C_{23} & 0 & C_{25} & 0 \\ & & C_{33} & 0 & C_{35} & 0 \\ & & & C_{44} & 0 & C_{46} \\ & & & & C_{55} & 0 \\ & & & & & C_{66} \end{pmatrix}, \quad (6)$$

whose values were reported in Table 4. Very few experimental data were reported in the scientific literature because suitable single crystals of phlogopite are rare, and many of these specimens are required for a complete characterization of the elastic tensor of low-symmetry phases. Nevertheless, the present simulations were in good agreement with the experimental results of Alexandrov and Ryzhova (1961) and Aleksandrov et al. (1974), even if the cited authors considered phlogopite belonging to the hexagonal crystal system. In detail, the calculated trends of the diagonal components were $C_{11} \approx C_{22} > C_{33}$ and $C_{44} \approx C_{55} < C_{66}$, which are the same as those experimentally obtained from elastic wave propagation experiments (Aleksandrov et al., 1974; Alexandrov and Ryzhova, 1961). Also, the off-diagonal components were $C_{12} > C_{13} \approx C_{23}$, which is in line with the experimental evidence. For symmetry reasons, no experimental results on the off-diagonal components C_{15} , C_{25} , C_{35} and C_{46} were reported, hence no direct comparison was possible. The present results at the B3LYP-D* level of theory were also in very good agreement the simulations performed using the PAW/GGA approach of Chheda and co-workers (2014). In general, the elastic properties obtained from Gaussian-type orbitals basis sets are slightly larger than those resulting from the simulations with plane-waves basis sets in density functional theory simulation, and also from experimental elastic moduli.



210 As previously explained (Ulian et al., 2021;Ulian and Valdrè, 2018), this overestimation is systematic and due to (i) the
absence of any thermal effect in the calculation and (ii) the Pulay forces that arise from the Hellmann-Feynman theorem and
the use of atom-centred (i.e., localized) Gaussian-type orbital basis sets.

215 **Table 4. Elastic moduli C_{ij} (in GPa) of phlogopite polytypes obtained in the present DFT simulations, compared to previous
theoretical and experimental data.**

	GTO/B3LYP-D* ^a	GTO/B3LYP-D* ^a	PAW/LDA ^b	PAW/GGA ^b	EWP ^c	EWP ^c
Polytype	1M	2M ₁	1M	1M	1M	1M
P (GPa)	0.05	0.05	0	0	0	0
C_{11}	213.06	215.21	199.5	181.2	179	178
C_{22}	216.5	215.93	201.2	184.7	179	178
C_{33}	74.39	76.94	82.2	62.1	51.7	51
C_{44}	19.78	16.92	17	13.5	5.6	6.5
C_{55}	21.84	20.07	25.3	20	5.6	6.5
C_{66}	80.86	85.04	72.4	67.9	73.3	73.6
C_{12}	48.38	49.91	54.1	47.6	32.4	30.2
C_{13}	27.03	25.69	25.4	12.2	25.8	15.2
C_{23}	25.05	22.29	24.4	12.1	25.8	15.2
C_{15}	-23.34	-17.81	-13.1	-15.7	-	-
C_{25}	-7.23	0.87	-4.5	-4.9	-	-
C_{35}	2.88	1.55	-2.8	-1.2	-	-
C_{46}	-14.86	-2.33	-6.4	-5.9	-	-

Notes: GTO – Gaussian-type orbitals; PAW – projector-augmented wave; EWP – Elastic wave propagation. a – present work; b – Chheda et al. (2014); c – Aleksandrov et al. (1974).

For practical applications, it is commonly preferred the use of the polycrystalline averages, namely the bulk (K) and shear (μ)
220 moduli, calculated with the Voigt–Reuss–Hill approach (Hill, 1952;Nye, 1957) according to the formulas:

$$K_V = (1/9)[C_{11} + C_{22} + C_{33} + 2(C_{12} + C_{13} + C_{23})] \quad (7)$$

$$K_R = [S_{11} + S_{22} + S_{33} + 2(S_{12} + S_{13} + S_{23})]^{-1} \quad (8)$$

$$\mu_V = \frac{[C_{11} + C_{22} + C_{33} + 3(C_{44} + C_{55} + C_{66}) - (C_{12} + C_{13} + C_{23})]}{15} \quad (9)$$

$$\mu_R = \frac{15}{4[S_{11} + S_{22} + S_{33} - (S_{12} + S_{13} + S_{23})] + 3(S_{44} + S_{55} + S_{66})} \quad (10)$$

225 where $S_{ij} = C_{ij}^{-1}$ are the component of the compliance tensor, i.e., the inverse of elastic moduli tensor \mathbf{C} , and the subscripts V
and R indicate the Voigt (upper) and Reuss (lower) bound of the isotropic elastic properties. The Young's modulus E and the
Poisson's ratio ν were calculated from the following relations:

$$E = \frac{9K\mu}{3K + \mu} \quad (11)$$

and

$$230 \quad \nu = \frac{3K - 2\mu}{2(3K + \mu)} \quad (12)$$



The polycrystalline mechanical properties were reported in Table 5. The K_R values obtained for both phlogopite $1M$ and $2M_1$ polytypes were 58.8 GPa and 59.4 GPa, respectively, which are consistent with those calculated through the BM3 fitting procedure (57.9 GPa and 58.3 GPa, respectively).

235 **Table 5. Isotropic elastic properties (bulk K , shear μ , and Young's E moduli, and Poisson's ratio ν) of phlogopite, alongside the universal anisotropy index A^U and the percentage of anisotropy of the bulk (A_K) and shear (A_μ) moduli.**

	GTO/B3LYP-D** ^a		PAW/LDA ^b	PAW/GGA ^b	Experimental ^{c,†}
	$1M$	$2M_1$	$1M$	$1M$	$1M$
K_V (GPa)	78.3	78.2	77.2	61.0	64.2
K_R (GPa)	58.8	59.4	62.9	43.0	45.4
μ_V (GPa)	51.4	51.8	47.6	43.3	38.6
μ_R (GPa)	30	30.6	31.2	24.1	11.8
E_V (GPa)	126.5	127.2	-	-	96.5
E_R (GPa)	77.0	78.4	-	-	32.5
ν_V	0.231	0.229	-	-	0.250
ν_R	0.282	0.280	-	-	0.381
A^U	3.90	3.78	2.86 [†]	4.40 [†]	11.77
A_K (%)	14.22	13.66	10.21 [†]	17.31 [†]	17.15
A_μ (%)	26.29	25.73	20.81 [†]	28.49 [†]	53.17

a – present work; b – Chheda et al. (2014); c – Aleksander et al. (1974). Subscripts V and R indicate the Voigt (upper) and Reuss (lower) bounds, respectively. [†]Values calculated in the present work from the second-order elastic moduli reported by Aleksander et al. (1974).

240 The elastic anisotropy of phlogopite was described using the universal anisotropic index, A^U , as proposed by Ranganathan and Ostoja-Starzewski (2008):

$$A^U = 5 \frac{\mu_V}{\mu_R} + \frac{K_V}{K_R} - 6 \geq 0. \quad (13)$$

For all but isotropic systems, for which $A^U = 0$, the ratio between the Voigt and Reuss moduli is not equal to unity, thus $A^U > 0$. The percentage anisotropy in compression (A_K) and shear (A_μ) was also calculated according to the following formulas:

$$A_K = 100 \frac{K_V - K_R}{K_V + K_R} \quad (14)$$

$$A_\mu = 100 \frac{\mu_V - \mu_R}{\mu_V + \mu_R}$$

245 The anisotropies obtained via these expressions were reported in Table 5, showing that the A^U values of the two phlogopite polytypes are very similar (about 3.8), and between the values calculated from the theoretical results of Chheda and collaborators (2014) using the LDA (2.9) and GGA (4.4) functionals. There is a slight discrepancy between the different DFT approaches and the experimental results ($A^U = 11.8$), which is related to the high anisotropy of the shear moduli. It is suggested that the high μ_V/μ_R ratio is probably due to the very small values of the $C_{44} = C_{55}$ elastic tensor components that were experimentally measured by Aleksandrov et al. (1974) with elastic wave propagation methods. Similar figures were found for the bulk and shear anisotropies, with $A_K \approx 14\%$ and $A_\mu \approx 26\%$ calculated at the B3LYP-D* level of theory, 250 intermediate values between those obtained using LDA and GGA functionals by Chheda and co-workers (2014).



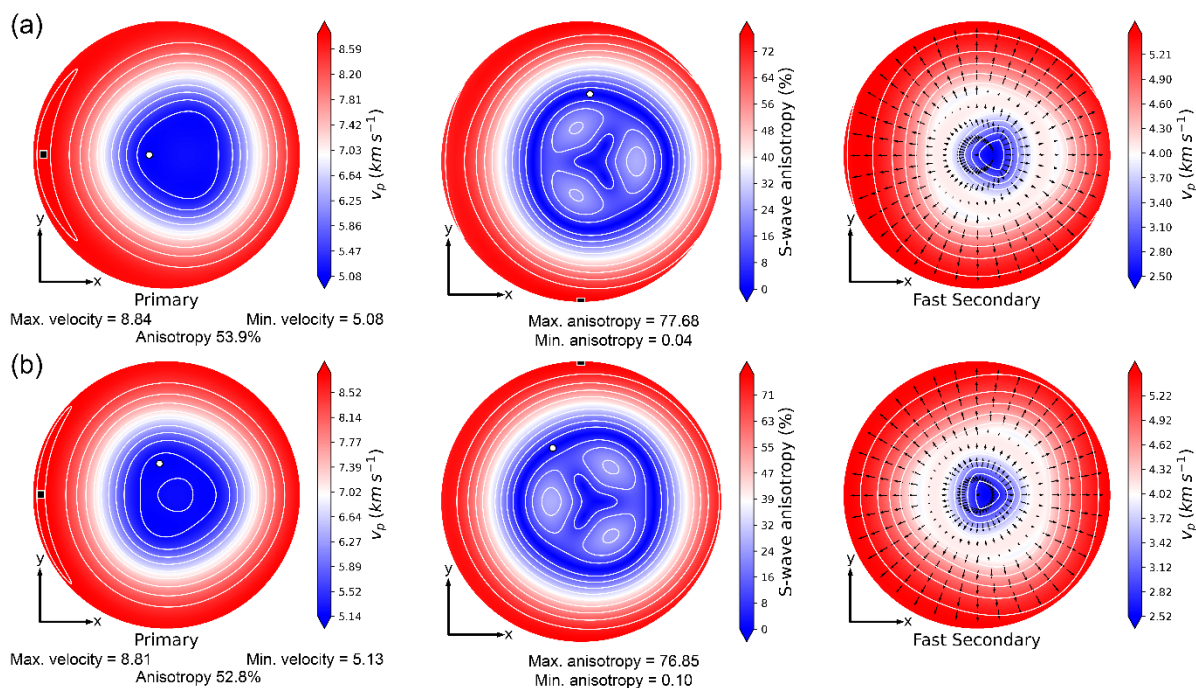
To further assess the validity of the linear model used to calculate the axial compressibilities, the axial moduli $M(a)$, $M(b)$ and $M(c)$ were calculated from the elastic compliance tensor components according to the expressions reported by Mookherjee et al. (2016):

$$\begin{aligned}M(a) &= \beta_a^{-1} = (S_{11} + S_{12} + S_{13})^{-1} \\M(b) &= \beta_c^{-1} = (S_{12} + S_{22} + S_{23})^{-1} \\M(c) &= \beta_c^{-1} = (S_{13} + S_{23} + S_{33})^{-1}\end{aligned}\tag{15}$$

The calculated moduli were $M(a) = 344.3$ GPa, $M(b) = 365.2$ GPa and $M(c) = 88.0$ GPa for phlogopite-1M, and $M(a) = 360.5$ GPa, $M(b) = 353.9$ GPa and $M(c) = 89.1$ GPa for the $2M_1$ polytype, values consistent with those reported in Table 3 obtained from the equation of state fit and that provide another measure of the anisotropy of the mineral, with a ratio $M(a) : M(b) : M(c) \approx 4 : 4 : 1$ for both polytypes.

Directional single-crystal elastic properties (Young's modulus E , linear compressibility $\beta = K^{-1}$, shear modulus μ and Poisson's ratio ν) were calculated in the Cartesian space using the QUANTAS code (Gaillac et al., 2016; Ulian and Valdrè, 2022). The interested reader can find in the cited works all the formulations employed to calculate the spatial dependence of the cited properties. Differently from the other elastic properties reported above, where no significant variation between the 1M and $2M_1$ phlogopite polytypes was evinced, the directional properties showed some effect due to the different TOT stacking (see Fig.S1 in the Supplementary Materials). For example, the shape of the Young's modulus on the (xy) plane (Fig.S1a) is slightly more compressed along NE-SW and NO-SE directions in the polytype-1M, while it appeared more isotropic in phlogopite- $2M_1$. The shear moduli on the (xz) plane of the latter polytype (see Fig.S1c) is slightly canted, with the oblate maxima direction almost parallel to the east-west direction.

Finally, the phase (seismic) velocities were calculated by solving Christoffel's equation (Musgrave, 1970) using the routines implemented in the QUANTAS code (Jaeken and Cottenier, 2016; Ulian and Valdrè, 2022). The results are shown in Fig.4, where the compressional wave velocity (v_p , P-wave, primary), the anisotropy of the shear velocities (S-wave, secondary), and the polarization of the fast shear wave (v_{SI}) are reported for both phlogopite polytypes. From the stereographic projections, particularly the S-wave anisotropy, it is immediately visible an east-ovest mirror plane normal to the b-axis that is related to the monoclinic crystal system of the mineral. This figure is in very good agreement with the theoretical analysis of Chheda et al. (2014), with some degree of deviation of the absolute values of the seismic velocities and anisotropy due to the stiffer elastic moduli obtained with the combination of the Gaussian-type orbitals basis sets and hybrid B3LYP-D* functional.



285 **Figure 4. Lamber equal area (stereographic) projection of the upper hemisphere of the seismic anisotropy calculated for (a) 1M and (b) 2M₁ polytypes of phlogopite. In each panel, the left picture is related to the primary velocity, the central one is the S-wave anisotropy (related to the fast and slow shear waves) and the rightmost stereoplot is the polarization of the v_{s1} (fast secondary) shear velocity. All the quantities were calculated at the DFT/B3LYP-D* level of theory.**

4. Conclusions

290 In the present work, using ab initio Density Functional Theory simulations, the elastic properties of two phlogopite polytypes, namely the 1M and the 2M₁, were investigated considering hydrostatic compression up to about 15 GPa and the monoclinic elastic tensor. The following conclusions can be drawn:

- (1) despite the different stacking of the TOT layers, the elastic properties of phlogopite were not severely affected by polytypism. Considering the numerical errors of the fitting procedure, the bulk modulus K_0 obtained from the third-order Birch-Murnaghan equation of state was in the range 55 – 60 GPa for both polytypes.
- 295 (2) the compressional behaviour of phlogopite is highly anisotropic, with the **a** and **b** crystallographic axes being about four times less compressible than the **c** one, as noticed from the linear moduli. This agrees with the experimental observations made on dioctahedral and trioctahedral micas, and it is due to several factors, i.e., the high compressibility of the interlayer region, the low compressibility of the tetrahedral and octahedral polyhedral, and the accommodation of the stress within the TOT layers via variation of the tetrahedral rotation angle α_r .



300 (3) the elastic tensors of phlogopite-1M and phlogopite-2M₁ have comparable C_{ij} components (in Voigt's notation), with a difference in sign and absolute value in the C_{25} one. This is probably the reason of the small differences observed in the directionally dependent elastic properties.

(4) the DFT simulations were able to correctly describe the behaviour of the known 1M polytype of phlogopite, extending the knowledge to the 2M₁ one. In particular, the use of the DFT-D2 correction provided a robust description of the physical
305 forces acting along [001], namely the stacking direction of the TOT + i layers.

It is also known that the elastic properties of micas can be deeply affected by the presence of cationic/anionic substitutions in the T and O sheets, e.g., Fe^{II} substituting Mg^{II}. These are currently under investigation and will be the subject of a future work.

310 **Acknowledgements**

The authors wish to thank the University of Bologna for supporting the present research. All the simulations were performed with the computational resources (HPC cluster) and software license of the Interdisciplinary Research Centre of Biomineralogy, Crystallography and Biomaterials, Department of Biological, Geological and Environmental Sciences, University of Bologna.

315

Competing Interests

The authors declare that they have no known competing financial interests or personal relationships that could have appeared to influence the work reported in this paper.

320 **Author Contributions**

Conceptualization, G.U. and G.V.; methodology, G.U. and F.R.; validation, G.U. and G.V.; formal analysis, G.U.; investigation, G.U. and G.V.; data curation, G.U. and F.R.; writing—review and editing, G.U., F.R. and G.V.; visualization, G.U. and F.R.; supervision, G.V. All authors have read and agreed to the published version of the manuscript.

325 **Data Availability**

The results of the present work are reported in the manuscript and in a dedicated dataset published at the following link:
<https://doi.org/10.17632/r4wmxz7kcc.1>.

References

Aleksandrov, K. S., Alchikov, U. V., Belikov, B. P., Zaslavskii, B. I., and Krupnyi, A. I.: Velocities of elastic waves in
330 minerals at atmospheric pressure and increasing precision of elastic constants by means of EVM [in Russian]. In: *Izv. Acad. Sci. USSR, Geol. Ser.*, 1974.



- Alexandrov, K. S., and Ryzhova, T. V.: Elastic properties of rock-forming minerals. II. Layered silicates, *Bulletin of the Academy of Sciences of the U.S.S.R, Geophysics Series*, 9, 1165-1168, 1961.
- Angel, R. J., Gonzalez-Platas, J., and Alvaro, M.: EosFit7c and a Fortran module (library) for equation of state calculations, *Zeitschrift Fur Kristallographie*, 229, 405-419, 10.1515/zkri-2013-1711, 2014.
- 335 Ariane, K., Tamayo, A., Chorfa, A., Rubio, F., and Rubio, J.: Optimization of the nucleating agent content for the obtaining of transparent fluormica glass-ceramics, *Ceramics International*, 49, 9826-9838, 10.1016/j.ceramint.2022.11.156, 2023.
- Becke, A. D.: Density-Functional Thermochemistry .3. The Role of Exact Exchange, *Journal of Chemical Physics*, 98, 5648-5652, 10.1063/1.464913, 1993.
- 340 Belmonte, D.: First Principles Thermodynamics of Minerals at HP-HT Conditions: MgO as a Prototypical Material, *Minerals*, 7, 183, 10.3390/Min7100183, 2017.
- Birch, F.: Finite elastic strain of cubic crystal, *Physical Review*, 71, 809-824, 1947.
- Broyden, C. G.: The convergence of a class of double-rank minimization algorithms: 2. The new algorithm, *IMA Journal of Applied Mathematics*, 6, 222-231, 10.1093/imamat/6.3.222, 1970a.
- 345 Broyden, C. G.: The convergence of a class of double-rank minimization algorithms: 1. General considerations, *IMA Journal of Applied Mathematics*, 6, 76-90, 10.1093/imamat/6.1.76, 1970b.
- Catti, M., Ferraris, G., Hull, S., and Pavese, A.: Powder Neutron-Diffraction Study of $2M_1$ Muscovite at Room Pressure and at 2 Gpa, *European Journal of Mineralogy*, 6, 171-178, 1994.
- Chheda, T. D., Mookherjee, M., Mainprice, D., dos Santos, A. M., Molaison, J. J., Chantel, J., Manthilake, G., and Bassett, W. A.: Structure and elasticity of phlogopite under compression: Geophysical implications, *Physics of the Earth and Planetary Interiors*, 233, 1-12, 10.1016/j.pepi.2014.05.004, 2014.
- 350 Civalleri, B., Zicovich-Wilson, C. M., Valenzano, L., and Ugliengo, P.: B3LYP augmented with an empirical dispersion term (B3LYP-D*) as applied to molecular crystals, *CrystEngComm*, 10, 405-410, 10.1039/b715018k, 2008.
- Comodi, P., and Zanazzi, P. F.: High-Pressure Structural Study of Muscovite, *Physics and Chemistry of Minerals*, 22, 170-177, 1995.
- 355 Comodi, P., Fumagalli, P., Montagnoli, M., and Zanazzi, P. F.: A single-crystal study on the pressure behavior of phlogopite and petrological implications, *American Mineralogist*, 89, 647-653, 10.2138/am-2004-0420, 2004.
- Donnay, G., Morimoto, N., and Takeda, H.: Trioctahedral one-layer micas. II. Prediction of the structure from composition and cell dimensions, 17, 1374-1381, <https://doi.org/10.1107/S0365110X64003462>, 1964a.
- 360 Donnay, G., Morimoto, N., and Takeda, H.: Trioctahedral one-layer micas. I. Crystal structure of a synthetic iron mica, 17, 1369-1373, <https://doi.org/10.1107/S0365110X64003450>, 1964b.
- Dovesi, R., Roetti, C., Freyria Fava, C., Prencipe, M., and Saunders, V. R.: On the elastic properties of lithium, sodium an potassium oxide. An ab initio study., *Chemical Physics*, 156, 11-19, 1991.



- Dovesi, R., Erba, A., Orlando, R., Zicovich-Wilson, C. M., Civalleri, B., Maschio, L., Rerat, M., Casassa, S., Baima, J.,
365 Salustro, S., and Kirtman, B.: Quantum-mechanical condensed matter simulations with CRYSTAL, Wiley Interdisciplinary
Reviews-Computational Molecular Science, 8, E1360, 10.1002/Wcms.1360, 2018.
- Fletcher, R.: A new approach to variable metric algorithms, The Computer Journal, 13, 317-322, 10.1093/comjnl/13.3.317,
1970.
- Gaillac, R., Pullumbi, P., and Coudert, F. X.: ELATE: an open-source online application for analysis and visualization of
370 elastic tensors, Journal of Physics-Condensed Matter, 28, 275201, 10.1088/0953-8984/28/27/275201, 2016.
- Gatta, G. D., Merlini, M., Rotiroti, N., Curetti, N., and Pavese, A.: On the crystal chemistry and elastic behavior of a
phlogopite 3T, Physics and Chemistry of Minerals, 38, 655-664, 10.1007/s00269-011-0438-z, 2011.
- Gatta, G. D., Lotti, P., Merlini, M., Liermann, H.-P., Lausi, A., Valdrè, G., and Pavese, A.: Elastic behaviour and phase
stability of pyrophyllite and talc at high pressure and temperature, Physics and Chemistry of Minerals, 42, 309-318,
375 10.1007/s00269-014-0721-x, 2015.
- Gatti, C., Saunders, V. R., and Roetti, C.: Crystal-field effects on the topological properties of the electron-density in
molecular-crystals - the case of urea, Journal of Chemical Physics, 101, 10686-10696, 10.1063/1.467882, 1994.
- Goldfarb, D.: A family of variable-metric methods derived by variational means, Mathematics of Computation, 24, 23-26,
10.1090/S0025-5718-1970-0258249-6 1970.
- 380 Hebbache, M., and Zemzemi, M.: Ab initio study of high-pressure behavior of a low compressibility metal and a hard
material: Osmium and diamond, Physical Review B, 70, 10.1103/Physrevb.70.224107, 2004.
- Hill, R.: The elastic behaviour of a crystalline aggregate, Proceedings of the Physical Society, London, Section A, 65, 349-
354, 1952.
- Icenhower, J., and London, D.: An experimental study of element partitioning among biotite, muscovite, and coexisting
385 peraluminous silicic melt at 200 MPa (H₂O), American Mineralogist, 80, 1229-1251, 10.2138/am-1995-11-1213, 1995.
- Jaeken, J. W., and Cottenier, S.: Solving the Christoffel equation: Phase and group velocities, Computer Physics
Communications, 207, 445-451, 10.1016/j.cpc.2016.06.014, 2016.
- King, T. T., Grayeski, W., and Cooper, R. F.: Thermochemical reactions and equilibria between fluoromicas and silicate
matrices: A petromimetic perspective on structural ceramic composites, Journal of the American Ceramic Society, 83, 2287-
390 2296, 10.1111/j.1151-2916.2000.tb01549.x, 2000.
- Lacalamita, M., Mesto, E., Scordari, F., and Schingaro, E.: Chemical and structural study of 1M- and 2M (1)-phlogopites
coexisting in the same Kasenyi kamafugitic rock (SW Uganda), Physics and Chemistry of Minerals, 39, 601-611,
10.1007/s00269-012-0515-y, 2012.
- Laurora, A., Brigatti, M. F., Mottana, A., Malferrari, D., and Caprilli, E.: Crystal chemistry of trioctahedral micas alkaline
395 and subalkaline volcanic rocks: A case study from Mt. Sassetto (Tolfa district, central Italy), American Mineralogist, 92,
468-480, 10.2138/am.2007.2339, 2007.



- Lee, C. T., Yang, W. T., and Parr, R. G.: Development of the Colle-Salvetti Correlation-Energy Formula into a Functional of the Electron-Density, *Physical Review B*, 37, 785-789, 10.1103/PhysRevB.37.785, 1988.
- Momma, K., and Izumi, F.: VESTA: a three-dimensional visualization system for electronic and structural analysis, *J. Appl. Crystallogr.*, 41, 653-658, 2008.
- Mookherjee, M., Tsuchiya, J., and Hariharan, A.: Crystal structure, equation of state, and elasticity of hydrous aluminosilicate phase, topaz-OH ($\text{Al}_2\text{SiO}_4(\text{OH})(2)$) at high pressures, *Physics of the Earth and Planetary Interiors*, 251, 24-35, 10.1016/j.pepi.2015.11.006, 2016.
- Musgrave, M. J. P.: *Crystal Acoustics: introduction to the study of elastic waves and vibrations in crystals*, Holden-Day, San Francisco, CA, USA, 1970.
- Nada, R., Nicholas, J. B., McCarthy, M. I., and Hess, A. C.: Basis sets for ab initio periodic Hartree-Fock studies of zeolite/adsorbate interactions: He, Ne, and Ar in silica sodalite, *International Journal of Quantum Chemistry*, 60, 809-820, 10.1002/(SICI)1097-461X(1996)60:4<809::AID-QUA3>3.0.CO;2-0, 1996.
- Nye, J. F.: *Physical properties of crystals*, Oxford University Press, Oxford, 1957.
- Ottonello, G., Civalleri, B., Ganguly, J., Perger, W. F., Belmonte, D., and Zuccolini, M. V.: Thermo-chemical and thermo-physical properties of the high-pressure phase anhydrous B ($\text{Mg}_{14}\text{Si}_5\text{O}_{24}$): An ab-initio all-electron investigation, *American Mineralogist*, 95, 563-573, 10.2138/am.2010.3368, 2010.
- Pavese, A., Ferraris, G., Pischedda, V., and Mezouar, M.: Synchrotron powder diffraction study of phengite 3T from the Dora-Maira massif: P-V-T equation of state and petrological consequences, *Physics and Chemistry of Minerals*, 26, 460-467, DOI 10.1007/s002690050208, 1999.
- Pavese, A., Levy, D., Curetti, N., Diella, V., Fumagalli, P., and Sani, A.: Equation of state and compressibility of phlogopite by in-situ high-pressure X-ray powder diffraction, *European Journal of Mineralogy*, 15, 455-463, 10.1127/0935-1221/2003/0015-0455, 2003.
- Pawley, A. R., Clark, S. M., and Chinnery, N. J.: Equation of state measurements of chlorite, pyrophyllite, and talc, *American Mineralogist*, 87, 1172-1182, 2002.
- Perger, W. F., Criswell, J., Civalleri, B., and Dovesi, R.: Ab-initio calculation of elastic constants of crystalline systems with the CRYSTAL code, *Computer Physics Communications*, 180, 1753-1759, DOI 10.1016/j.cpc.2009.04.022, 2009.
- Pfrommer, B. G., Côté, M., Louie, S. G., and Cohen, M. L.: Relaxation of Crystals with the Quasi-Newton Method, *Journal of Computational Physics*, 131, 233-240, 10.1006/jcph.1996.5612, 1997.
- Prencipe, M., Noel, Y., Bruno, M., and Dovesi, R.: The vibrational spectrum of lizardite-1T [$\text{Mg}_3\text{Si}_2\text{O}_5(\text{OH})_4$] at the Gamma point: A contribution from an ab initio periodic B3LYP calculation, *American Mineralogist*, 94, 986-994, 2009.
- Ranganathan, S. I., and Ostoja-Starzewski, M.: Universal elastic anisotropy index, *Physical Review Letters*, 101, 055504, 10.1103/PhysRevLett.101.055504, 2008.
- Shanno, D. F.: Conditioning of quasi-Newton methods for function minimization, *Mathematics of Computation*, 24, 647-656, 10.1090/S0025-5718-1970-0274029-X 1970.



- Trønnes, R. G.: Stability range and decomposition of potassic richterite and phlogopite end members at 5-15 GPa, *Mineralogy and Petrology*, 74, 129-148, 10.1007/s007100200001, 2002.
- Tutti, F., Dubrovinsky, L. S., and Nygren, M.: High-temperature study and thermal expansion of phlogopite, *Physics and Chemistry of Minerals*, 27, 599-603, 10.1007/s002690000098, 2000.
- 435 Ulian, G., Tosoni, S., and Valdrè, G.: Comparison between Gaussian-type orbitals and plane wave ab initio density functional theory modeling of layer silicates: Talc $\text{Mg}_3\text{Si}_4\text{O}_{10}(\text{OH})_2$ as model system, *Journal of Chemical Physics*, 139, 204101, 10.1063/1.4830405, 2013.
- Ulian, G., and Valdrè, G.: Density functional investigation of the thermophysical and thermochemical properties of talc $\text{Mg}_3\text{Si}_4\text{O}_{10}(\text{OH})_2$, *Physics and Chemistry of Minerals*, 42, 151-162, 10.1007/s00269-014-0708-7, 2015a.
- 440 Ulian, G., and Valdrè, G.: Structural, vibrational and thermophysical properties of pyrophyllite by semi-empirical density functional modelling, *Physics and Chemistry of Minerals*, 42, 609-627, 10.1007/s00269-015-0748-7, 2015b.
- Ulian, G., and Valdrè, G.: Density functional investigation of the thermo-physical and thermo-chemical properties of 2M(1) muscovite, *American Mineralogist*, 100, 935-944, 10.2138/am-2015-5086, 2015c.
- Ulian, G., and Valdrè, G.: Second-order elastic constants of hexagonal hydroxylapatite (P_6_3) from ab initio quantum
445 mechanics: comparison between DFT functionals and basis sets, *International Journal of Quantum Chemistry*, 118, e25500, 10.1002/qua.25500, 2018.
- Ulian, G., and Valdrè, G.: Equation of state and second-order elastic constants of portlandite $\text{Ca}(\text{OH})_2$ and brucite $\text{Mg}(\text{OH})_2$, *Physics and Chemistry of Minerals*, 46, 101-117, 10.1007/s00269-018-0989-3, 2019.
- Ulian, G., Moro, D., and Valdrè, G.: Elastic properties of heterodesmic composite structures: The case of calcite CaCO_3
450 (space group R-3c), *Composites Part C: Open Access*, 6, <https://doi.org/10.1016/j.jcomc.2021.100184>, 2021.
- Ulian, G., and Valdrè, G.: QUANTAS, a Python software for the analysis of solids from ab initio quantum mechanical simulations and experimental data, *J. Appl. Crystallogr.*, 55, 386-396, 10.1107/S1600576722000085, 2022.
- Ulian, G., and Valdrè, G.: Crystal-chemical, vibrational and electronic properties of 1M-phlogopite
 $\text{K}(\text{Mg},\text{Fe})_3\text{Si}_3\text{AlO}_{10}(\text{OH})_2$ from Density Functional Theory simulations, *Applied Clay Science*, 246, 107166,
455 10.1016/j.clay.2023.107166, 2023a.
- Ulian, G., and Valdrè, G.: The effect of long-range interactions on the infrared and Raman spectra of aragonite (CaCO_3 , *Pmcn*) up to 25 GPa, *Scientific Reports*, 13, 2725, 10.1038/s41598-023-29783-7, 2023b.
- Ulian, G., and Valdrè, G.: SEISMIC, a Python-based code of the QUANTAS package to calculate the phase and group acoustic velocities in crystals, *Computers and Geosciences*, 188, 10.1016/j.cageo.2024.105615, 2024.
- 460 Valenzano, L., Noel, Y., Orlando, R., Zicovich-Wilson, C. M., Ferrero, M., and Dovesi, R.: Ab initio vibrational spectra and dielectric properties of carbonates: magnesite, calcite and dolomite, *Theoretical Chemistry Accounts*, 117, 991-1000, 10.1007/s00214-006-0213-2, 2007.

<https://doi.org/10.5194/egusphere-2024-3429>

Preprint. Discussion started: 15 January 2025

© Author(s) 2025. CC BY 4.0 License.



Ventruți, G., Levy, D., Pavese, A., Scordari, F., and Suard, E.: High-temperature treatment, hydrogen behaviour and cation partitioning of a Fe-Ti bearing volcanic phlogopite by in situ neutron powder diffraction and FTIR spectroscopy, *European Journal of Mineralogy*, 21, 385-396, 10.1127/0935-1221/2009/0021-1903, 2009.

465

Virgo, D., and Popp, R. K.: Hydrogen deficiency in mantle-derived phlogopites, *American Mineralogist*, 85, 753-759, 10.2138/am-2000-5-614, 2000.